Segmentation of Cracks in X-ray CT Images of Tested Macroporous Plaster Specimens

Ujjal Kumar Bhowmik
Electrical Engineering and Computer Science Dept.
Catholic University of America, Washington DC, USA
Email: bhowmik@cua.edu

Divya Mandala, Nick W. Hudyma, O. Patrick Kreidl, and Alan Harris, School of Engineering,
University of North Florida
Jacksonville, FL-32224, USA

***Abstract*— Precise segmentation of cracks is essential to characterize the structural properties of a rock specimen under compressive force. A two-dimensional internal cross-sectional image of rock can be created using X-ray computed tomography (CT scanning). Cracks in rocks usually have very poor local contrast which makes it difficult to detect and segment cracks from the background using existing popular edge detection algorithms. In this paper, we propose a two-dimensional matched filtering technique followed by local entropy based thresholding, morphological operators and length filtering to detect and segment cracks from the cross-sectional images of rock. The proposed algorithm is tested on several macroporous plaster specimens. Experimental results demonstrate the effectiveness and robustness of the algorithm compared to hand-labeled ground truth segmentations.**

Keywords—Computed tomography; Edge detection, matched filtering, local entropy thresholding, mathematical morphology.

I. INTRODUCTION

It is well established that pores inside of rock, regardless of size, shape and location, have detrimental effects on strength and stiffness. In order to investigate these effects of porosity, rock specimens can be tested under compressive force in a universal testing machine. When the applied force exceeds the limiting point of the specimen, breaks and cracks will appear. Taking images of this internal structure, and then segmenting each image to identify the cracks from the background, can help characterize the nature of cracks and their relationship to pores. Computed tomography (CT), a widely used non-invasive medical imaging technology, is one approach to creating cross-sectional images of a rock specimen under investigation. However, segmenting cracks from the CT images is a challenging task.

Automatic detection and segmentation of cracks can be categorized as a problem of edge detection in image processing. Most generalized edge detection algorithms [1-10] do not take account of special properties of the object being detected, which in the case of cracks is that its two edges always run parallel to each other. Such objects may be represented by piece-wise linear segments of finite width. Direction gradients of these lines can be 180^0 apart and hence sometimes they are denoted as anti-parallels. Linear feature detection and extraction algorithm [11] extracts such object by identifying anti-parallels and tracking them along their gradient direction. This method produces excellent results for segmenting roads, rivers and geological images that appear with high contrast in most mapping imagery. However, in CT images of rock specimens, the contrast level between the cracks and the background is usually too low for these methods to work reliably without fragmenting the cracks.

In medical imaging, a body of research has developed to detect and segment blood vessels from retinal images [12-19]. Blood vessels in retinal images are similar in nature to the cracks in X-ray CT images of rock cross-section (Figure 1). In this paper, a 2-D Gaussian matched filtering technique described in [17] for blood vessels is used to enhance the crack from the background in CT images of rocks. The success of the technique depends upon proper choice of a threshold to distinguish the enhanced crack from the background. This can be accomplished via a local entropy based thresholding scheme [18,19], which considers the spatial distribution of gray levels in the image yet also preserves sufficient structural details of the image. It can still be difficult to distinguish between so-called micro-pores and the crack, particularly hairline cracks for which the inherent tradeoff between the entropy-based filter's sensitivity and the image's signal-to-noise ratio limits success. Thus, a final stage of our segmentation process is to combine morphological operators and a length filtering scheme to segment the cracks accurately.

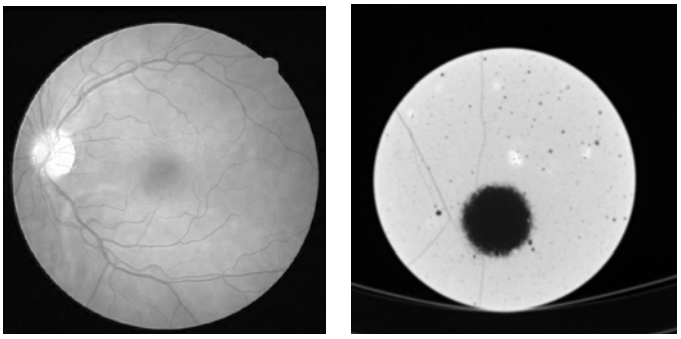

Figure 1. Retinal image (left), Rock cross-section (right)

The organization of the paper is as follows. Section II briefly describes the rock specimen and the CT scanning mode used in this research. Section III describes some special properties of cracks and a review of matched filtering detection. In Section IV, the mathematical formulation of local entropy based thresholding is given. Section V describes the morphological operators and length filtering schemes. Experimental results are given in section VI and Section VII discusses briefly area for further research. Section VIII concludes the paper.

II. CT SCANNING AND THE TEST SPECIMEN

Computer Tomography (CT), invented in 1972 by G.M. Hounsfield and A. Cormack, is an imaging technology to create cross-sectional image of an object from a set of X-ray projections taken around the objects. The process of creating the cross-section image from X-ray projection is called reconstruction [20]. Over the last decade CT technology has advanced tremendously, now we can create three-dimensional images of internal part of an object [21].

The test specimens used in this research were made from plaster of paris (Figure 2) which contained regularly shaped Styrofoam inclusions. Seven test specimens, as listed in Table 1, were used for this study. Styrofoam inclusions were meant to represent the macropores in the rock [22]. The specimens were designed to include a variety of simple macropore shapes, a variety of similarly sized macropores, and a variety macropores with the same shape but different sizes. Each of these test specimens was put on a universal testing machine and a compressive force was applied until it reached to its break point. Then these seven specimens were taken to the UF-SHANDS Health Science Center in Jacksonville Florida for CT scanning. This facility is a major academic medical center associated with the University of Florida which provides advanced medical treatment and research facilities. For this study, a 64-slice, dual X-ray tube medical CT scanner (Definition Dual Source, Siemens Medical Solutions, Forchheim, Germany) was used to obtain gold standard images for localization of cracks and volume measurement of the Styrofoam macropores. Specimens were positioned on the scanner bed such that the cylinders' Z (long) axes were aligned with that of the scanner. A helical scan protocol was used to obtain volumetric images as the specimens passed through the scanner gantry. Figure 3 shows the scanning operation for the CT imaging. Projection data were acquired using an X-ray tube energy of 120kV, tube current of 500mA, and exposure time of 500ms. Cross-sectional images were reconstructed at a slice thickness of 1mm with in-plane spatial resolution of 0.4 mm x 0.4 mm. Each cross-sectional image was saved in a DICOM (Digital Imaging and Communications in Medicine) file format. For each test specimen we saved 327 cross-sectional images. Couples of these cross-sectional images are shown in Figure 4. When theses cross-sectional images are stacked on top of one another and some interpolation technique is applied, the three-dimensional volumetric image of a test specimen can be created. As shown in Figure 5, a three-dimensional (3D) image of the internal structure of a portion of test specimen is created by using a commercially available visualization software program (Voxler by Golden Software). Different colors were chosen to make the cracks and macropores visible in the image. 3D segmentation is a computational intensive process. In this paper, we only propose a technique for segmentation of cracks from cross-section images of the test specimen. The whole idea is after completing 2D segmentation of cracks from all the cross-sections of a test specimen, we can stack them on top of another to get the 3D structure of cracks (future work). Following are the step by step methods for segmenting crack from a cross-section image of a test specimen.

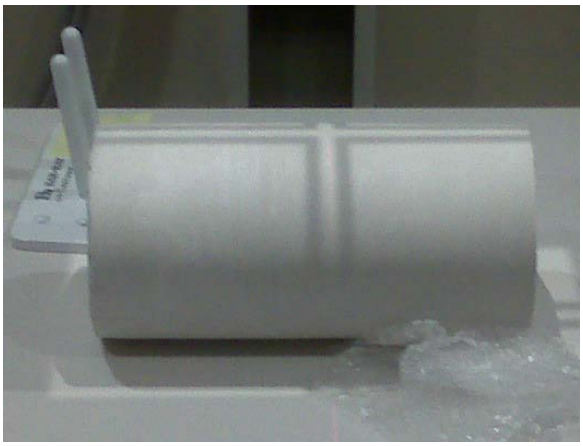

Figure 2. Plaster of Paris test specimen

Figure 3. CT scanning of plaster specimen

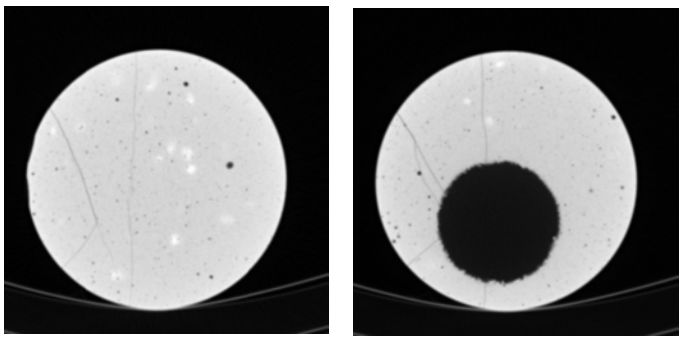

Figure 4. CT image of specimen cross-section

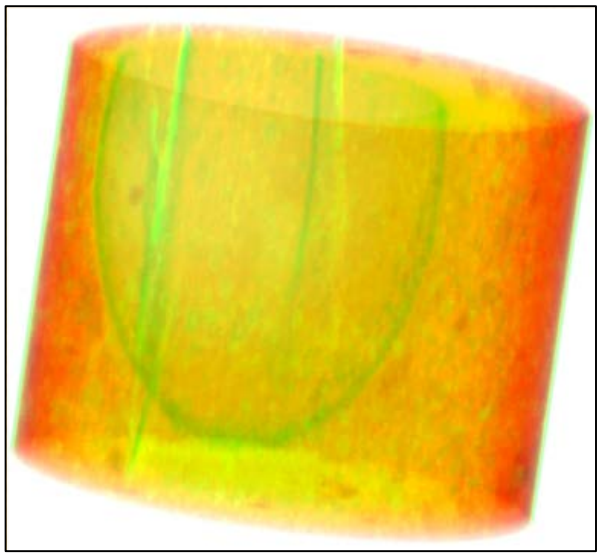

Figure 5. Partial volume of a test specimen.

Table 1. Description of test specimens

Specimen	Number of Styrofoam Macropores with Shapes and Dimensions	Total Macropore Volume (cm^3)
1	1 – 10.6 cm diameter sphere	938.5
	1 – 7.3 cm cube	
2	2 – 6.35 cm diameter spheres	511.6
	2 – 5.87 x 7.78 cm egg shapes	
3	6 – 5.08 cm diameter spheres	411.8
4	2 – 5.87 x 7.78 cm egg shapes	599.8
	2 – 7.62 x 5.08 cm cone shapes	
	2 – 6.35 cm diameter spheres	
5	10 – 2.54 cm cubes	249.7
	10 – 2.54 cm diameter spheres	
6	5 – 5.08 cm diameter spheres	536.2
	5 – 3.81 cm diameter spheres	
	5 – 2.54 cm diameter spheres	
	5 – 1.27 cm diameter spheres	
7	2 – 7.3 x 14.9 cm cones	435.9

III. MATCHED FILTER

It is observed that the cracks have lower reflectance relative to their neighbor and they appear darker compared to the background. It is also observed that the cracks almost never have ideal step edges (Figure 6). Because of crack's small curvature, the anti-parallel pair may be approximated by piece-wise linear segment. From the few representative samples of cracks' gray-level intensity profile along direction perpendicular to their length (as plotted in Figure 7), it becomes apparent that the cracks can be represented by an inverse Gaussian shaped curve [17],

$$g(x,y) = R\{1 - k\, e^{-d^2/2\sigma^2}\} \qquad (1)$$

where, d is the perpendicular distance between the point (x,y) and the straight line passing through the center of the crack in a direction along its length, R is the gray-level intensity of background, σ defines the spread of the intensity profile, and k is the measure of reflectance relative to its neighborhood. The width of a crack gradually changes as it travels along the cross-section. The widths of the cracks are found to be within the range of 2-8 pixels. For our initial calculation, we assume the width is of uniform length, 2σ.

Now, suppose we want to detect an arbitrary 1-D signal $z(t)$ in an additive Gaussian white noise. If the signal is passed through a filter with transfer function $H(f)$, the output signal $z_o(t)$ is given by [17]

$$z_o(t) = \int H(f)\{Z(f) + \eta(f)\}e^{j2\pi ft}df \qquad (2)$$

where $Z(f)$is the Fourier transform of $z(t)$, and $\eta(f)$ is the noise spectrum. The filter $H(f)$ that maximizes the output signal-to-noise ratio is given by, $H_{opt}(f) = Z^*(f)$. Since the input signal is of real valued, $h_{opt}(t) = z(-t)$. For our present context, intensity profile can be assumed to be symmetrical, i.e. $z(-t) = z(t)$. The optimal filter must have the same shape as the intensity profile itself. In other words, the optimal filter is given by, $h_{opt}(d) = -e^{-\frac{d^2}{2\sigma^2}}$. The negative sign indicates that cracks have darker values then the background.

The cracks usually have poor local contrast. In order to increase the local contrast of cracks, we need to extend matched filtering concept to 2D images. It must be noted that the crack may be oriented at any angle $\theta(0^0 \le \theta \le 180^0)$. The matched filter $z(t)$ will have maximum response at an angle $\theta \pm 90^0$. Thus, the filter needs to be rotated for all possible angles, the corresponding responses are to be compared, and the maximum response for each pixel is to be stored. For this research, we have rotated the filter with a step size of $\pm 7.5^0$.

The two-dimensional matched filter kernel is designed to convolve with the original cross-sectional image. The kernel of this filter is expressed as

$$f(x,y) = -e^{-\frac{x^2}{2\sigma^2}},\ \text{for } |y| \le L/2 \qquad (3)$$

where L is the length of the piece-wise linear segment for which the crack is assumed to have a fixed orientation. The direction of the crack is assumed to be aligned along y-axis. Here, we have applied a set of twenty four (since, the kernel is rotated by $\pm 7.5^0$) 8×7 pixels kernels on the original image and at each pixel only the maximum of their responses is retained. The effectiveness of this 2-D matched filtering is shown in Figure 10 (b). The original image, as shown in Figure 10 (a), has very low contrast compared to the background, and its matched-filter-output (MFO), Figure 10 (b), shows that the contrast level of cracks is significantly enhanced.

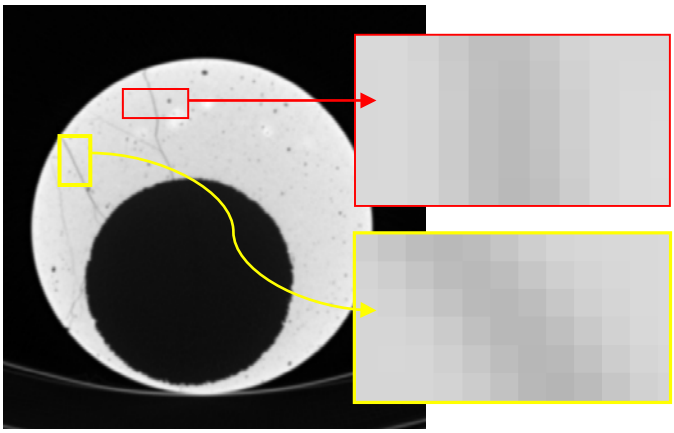

Figure 6. Cross-section of cracks showing gray level profile

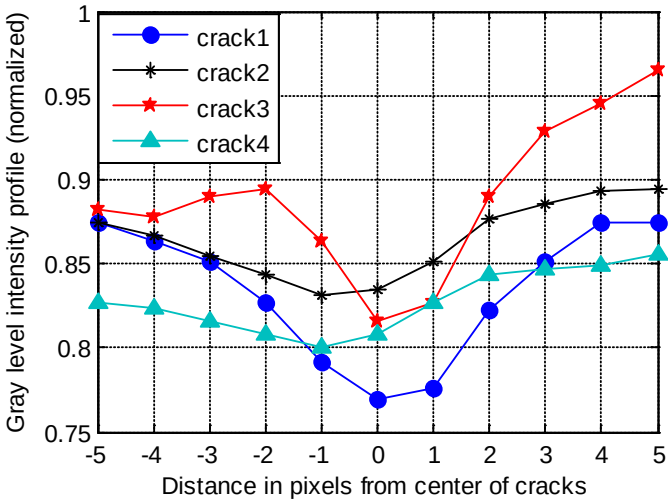

Figure 7. Gray-level intensity profile of cracks

IV. Local-Entropy Based Thresholding

In order to extract the cracks from background, the MFO image is processed by a proper thresholding value. An efficient local-entropy based thresholding algorithm [18], which is capable of preserving the spatial structures in the binarized/thresholded images, is used in this research. This algorithm takes in to account the spatial distribution of gray levels. As for example, two images with identical histograms but different spatial distributions will result in two different entropy values (in other words, will result in two different thresholding values).

In the following, we briefly describe the local-entropy based thresholding scheme. Let, $Q = |q_{ij}|_{m\times n}$ be an $m\times n$ dimensional co-occurrence matrix of an image of $f(l,k)$, which gives an idea about the transition of gray-level intensities (i, j) between the adjacent pixels. Thus, Q possesses the spatial structural information of an image. Depending upon the ways gray-level i follows gray-level j, different types of co-occurrence matrix are possible. For this research, we used an asymmetric co-occurrence matrix which has horizontally right and vertically lower transitions [19]. Thus, q_{ij} is expressed as follows:

$$q_{ij} = \sum_{l=1}^{m}\sum_{k=1}^{n} \delta \tag{3}$$

where $\delta = 1$ if $\begin{cases} f(l,k) = i \quad \text{and} \quad f(l,k+1) = j \\ \text{or} \\ f(l,k) = i \quad \text{and} \quad f(l+1,k) = j \end{cases}$

$\delta = 0$ otherwise

The probability of co-occurrence p_{ij} of gray levels i and j can therefore be written as,

$$p_{ij} = \frac{q_{ij}}{\sum_i \sum_j q_{ij}} \tag{4}$$

If t, $0 \le t \le L-1$, is a threshold. Then t can partition the co-occurrence matrix into four quadrants, namely A, B, C and D (Figure 8).

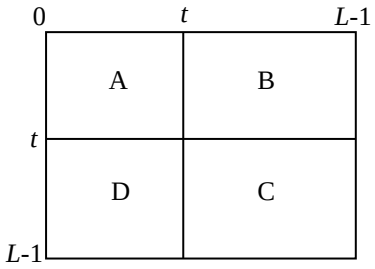

Figure 8. Quadrants of co-occurrence matrix

Let us define the probabilities of quadrants A and C as,

$$P_A = \sum_{i=0}^{t}\sum_{j=0}^{t} p_{ij}$$

$$P_C = \sum_{i=t+1}^{L-1}\sum_{j=t+1}^{L-1} p_{ij} \tag{5}$$

Normalizing the probabilities within each quadrants, such that the sum of probabilities of each quadrant equals one, we get the following probabilities of each cell quadrants:

$$P_{ij}^{A} = \frac{p_{ij}}{P_A} = \frac{q_{ij}}{\sum_{i=0}^{t}\sum_{j=0}^{t} q_{ij}}$$

Similarly,

$$P_{ij}^{C} = \frac{p_{ij}}{P_C} = \frac{q_{ij}}{\sum_{i=t+1}^{L-1}\sum_{j=t+1}^{L-1} q_{ij}} \tag{6}$$

The plot of P_{ij}^{A} and P_{ij}^{C} for our test image is shown in Figure 9.

The second-order entropy of the object can be expressed as:

$$H_A(t) = -\frac{1}{2}\sum_{i=0}^{t}\sum_{j=0}^{t} P_{ij}^{A}\, log_2 P_{ij}^{A} \quad (7)$$

Similarly, the second-order entropy of the background can be expressed as:

$$H_C(t) = -\frac{1}{2}\sum_{i=t+1}^{L-1}\sum_{j=t+1}^{L-1} P_{ij}^{C}\, log_2 P_{ij}^{C} \quad (8)$$

Thus, the total second-order local entropy of the object and the background can be expressed as:

$$H_T(t) = H_A(t) + H_C(t) \quad (9)$$

The plot of total second-order entropy, $H_T(t)$, along with the entropies of object and background for different gray-level intensities is shown in Figure 8. The gray-level corresponding to the maximum of $H_T(t)$ can be used as an optimum threshold for crack-background classification. The results of application of this local-entropy based thresholding is shown in Figure 10 (c). It is clearly evident that local-entropy based thresholding scheme does a pretty good job in segmenting visible cracks from the background. However, it has also extracted some microporous like structure as cracks. In the following section we describe the steps we have taken to tackle this problem.

V. Morphological Operator and Length Filtering

Although the local-entropy based thresholding does a very good job in extracting even hair line cracks, it acquires a significant number of misclassified pixels. Empirically we have tested that increasing the threshold value (for example, for our test case the threshold value we got from local-entropy based method is 88, but if we use threshold value as 92) would dramatically reduce the number of misclassified pixels, but the price we have to pay is that the filter then can no longer extract the hair line cracks. Thus, changing the threshold value would not be a good option for our case. Here, our objective would be to extract a clean and complete crack structure by removing misclassified pixels. To remove the misclassified pixels, we need to first isolate the misclassified pixels from the crack. Morphological operator, especially erosion operator, would be a good choice for this case. A short description of the erosion operator is given below.

We define a two dimensional (2D) image whose range $[N_{min}, N_{Max}]$ as a functional $F : \mathbb{R}^2 \rightarrow [N_{min}, N_{Max}]$, and a 2D structuring element as a functional $B : \mathbb{R}^2 \rightarrow \boldsymbol{B}$ where $\boldsymbol{B}$ is the set of the neighborhood of the origin. In our application, we only consider structuring elements invariant by translation. We then define the basic erosion operator, with respect to the structuring element B with a scaling factor e, image F and point $M_0 \in \mathbb{R}^2$:

$$\epsilon_B^e(F)(M_0) = MIN_{M \in M_0 + e.B(M_0)}\big(F(M)\big); \quad (10)$$

where the structuring elements are $B_1 = \begin{bmatrix}1\\1\\1\end{bmatrix}$ and $B_2 = [1 \quad 1]$

In Figure 10 (d), it is clearly seen that the erosion operation has isolated the undesired objects from the thresholded image. Now to remove the isolated pixels, a connected neighborhood based length filtering scheme is used. Isolated smaller connected regions correspond to undesired objects. The length filtering tries to remove the eight conned regions which have less than some certain number of pixels. Figure 10 (e) shows that the length filtering has removed almost all the undesired objects from the thresholded image.

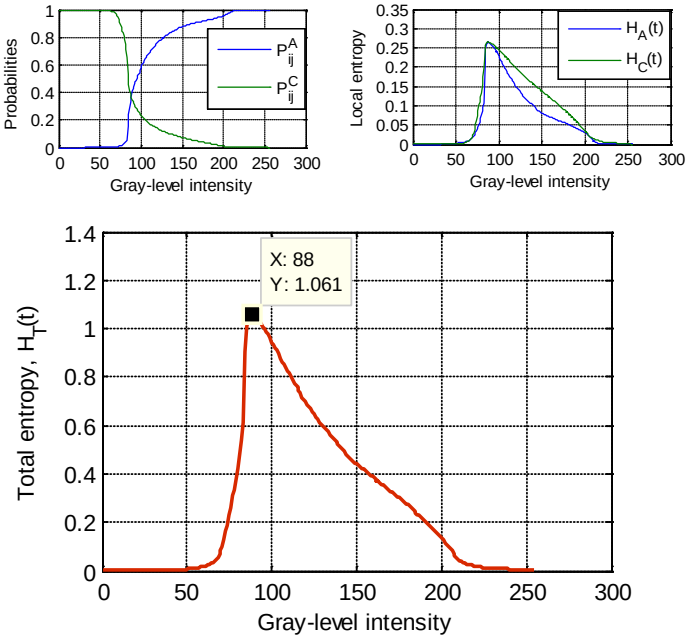

Figure 9. Plot of local-entropy Vs Gray -levels

VI. Experimental Results

We have tested our algorithm on seven different test specimens as mentioned in Table 1. Some of the test results are shown in Figure 10, 11, and 12. In Figure 10 (b-f), we show the results of every processing step of our algorithm. In Figure 10(b), it is clearly evident that the 2D matched filter has increased the local contrast of cracks. Choosing the proper size of the matched filter is critical. We empirically choose the piece wise linear segment of the crack, L = 8 pixels. Larger L would reduce the noise but it might not match well if the curve were quite tortuous in nature. From Figure 2, it is quite reasonable to choose the width of the curve as 7 pixels. Figure 10(c) shows the binary image acquired by local-entropy thresholding scheme. Although the binary image extracted complete crack structure (including the hair line structure on the lower left of the circular macrpore), it has also extracted a large number of misclassified pixels in the image. Thus, we

applied erosion operator to isolate the misclassified pixels from the cracks. Figure 10(d) shows that the undesired misclassified pixels are isolated from the curve structure and they become isolated smaller structure which can easily be removed by eight connected neighboring concept. Figure 10 (e & f) shows a clean complete segmented crack structure acquired by our length filtering step. In Figure 11 (a) we show the hand-labeled groundtruth segmentation which is labeled manually by us. Compared with the hand-label groundtruth, it can be inferred that our algorithm does a very good job in extracting clean and complete curve structure.

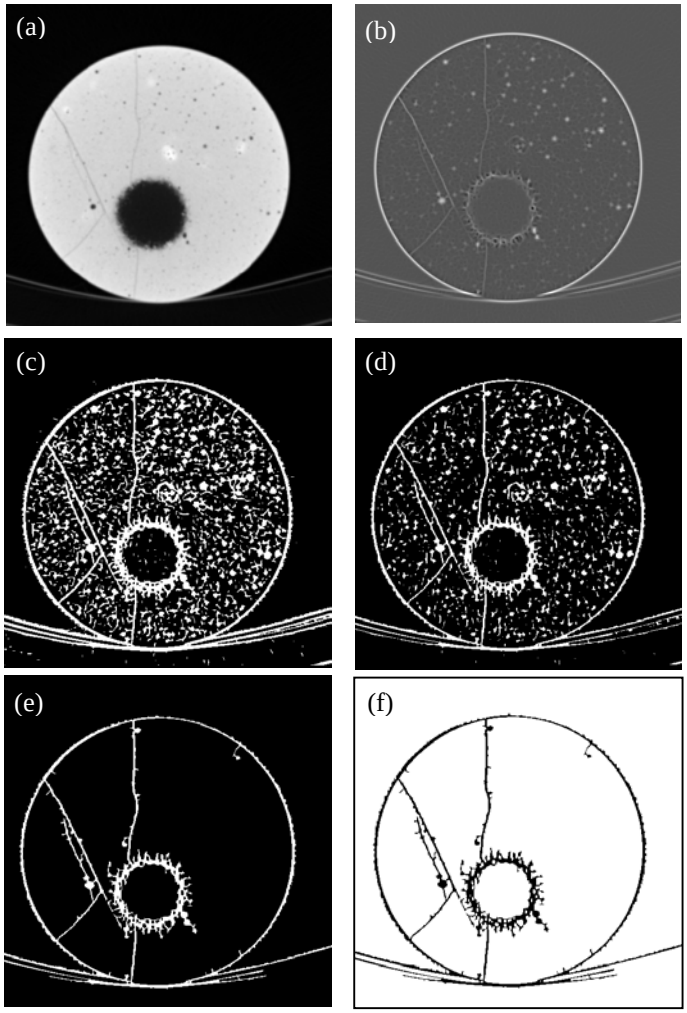

Figure 10. (a) Original cross-section, (b) Matched-filtered output, (c) Local-entropy based thresholding, (d) Erosion applied on thresholded image, (e) & (f) Output image after length filtering

To demonstrate the robustness of our algorithm, in Figure 12, we have showed the results we obtained from couples of abnormal images (where cracks are either much obscured or very tortuous). Figure 12 (a & b) shows that in case of nearly invisible crack lines our algorithm successfully extracted the cracks information. Although our algorithm performs very well, a significant improvement still be achieved in case of obscured and tortuous crack structure. To demonstrate the effect of choosing proper thresholding value on the signal-to-noise ratio and the sensitivity of our algorithm, we showed two different outcomes for the same image in Row 2 and 3 of Figure 12. Row 2 shows the output achieved by our algorithm following the steps we discussed. Although, it appears that our algorithm has produced a very good result, careful investigation of the original image (Figure 12 (c)) and matched filtered image (Figure 12 (e)) reveals the fact that our algorithm failed to extract a hair-line crack on the left side of squared macropore. As can be seen in Figure 12 (f), if we choose thresholding value a little smaller than the local-entropy thresholding value, we can recover that missed hair-line curve. But, the price we have to pay is some misclassified pixels are acquired in the binarized image. In our future endeavor, we expect to improve the robustness of our algorithm by considering pores information and including physical properties of the specimen.

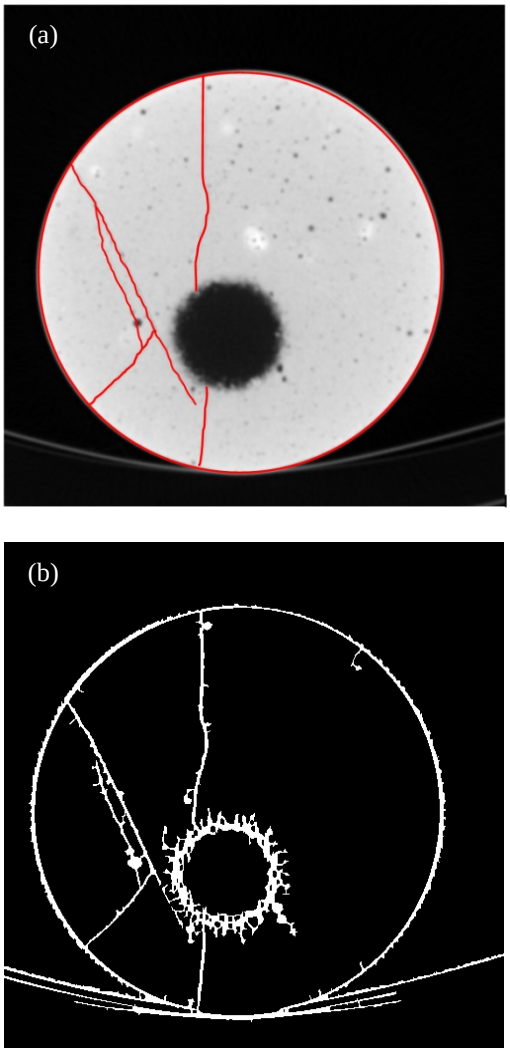

Figure 11. (a) Hand-labeled segmentation of cracks. (b) Segmentation produced by our algorithm

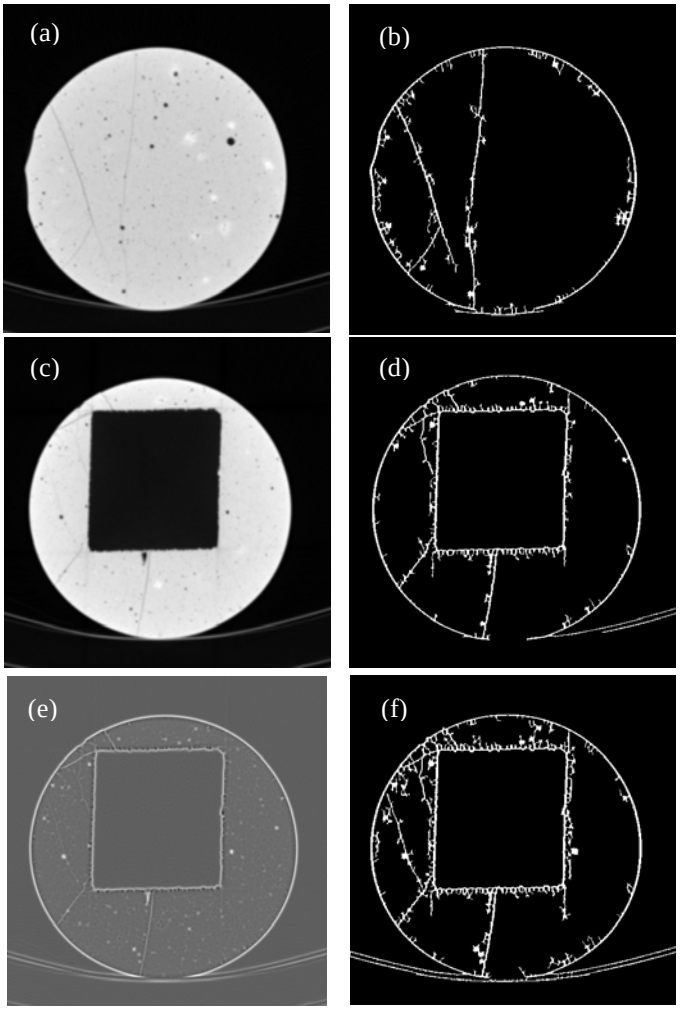

Figure 12. (a) Original cross-section, (b) Segmented image after applying our algorithm, (c) Original cross-section, (d) Corresponding segmented image after applying our algorithm, (e) Matched-filtered image of Fig.(c), (f) Segmentation with modified thresholding value.

VII. Challenges and Future Works

We are currently working on creating a fully automated 3D crack segmentation algorithm. Each test specimen has nearly 86 million data points (512*512*327). Dealing with such a large number of data points is a computationally intensive process. In order to create an efficient and faster segmentation technique, we are trying to implement our algorithm in the high performance computing facility (24 nodes GPU cluster) of Catholic University of America at Washington DC. Our ultimate objective is to superimpose the 3D segmented cracks on the 3D segmented macropores (in our previous work [22], [23], we have developed a band-pass filtering technique to segment macropore from the original image) and explore for a suitable mathematical model to find the strength and stiffness of the rock specimen in relation to its porosity, especially rock with large voids.

VIII. Conclusion

In this paper we have designed and implemented an effective crack segmentation algorithm to extract cracks from the cross-sectional images of rocks. The proposed algorithm consists of 2D matched filtering, local-entropy based thresholding, morphological operator and length filtering for extracting clean and complete crack structures. 2D matched filtering is used to enhance the cracks and entropy based thresholding is used to binarize the image while keeping the spatial structure of cracks. Morphological operator and the length filtering are used to remove the misclassified pixels from the binarized image. We have some issues with the sensitivity (especially, extracting hair-line cracks) and desired signal-to-noise ratio (removing misclassified pixels) of our algorithm. For some abnormal images our algorithm does not produce desired results. In the future work, more emphasis will be given to increase the robustness our algorithm.

Referenced

[1] I. E. Abdou and W. K. Pratt, "Quantitative design and evaluation of Enhancement/thresholding edge detectors," Proc. IEEE, vol. 67, pp. 753-763, May 1979.

[2] W. K. Pratt, Digital Image Processing.

[3] R. M. Haralick, J. S. J. Lee, and L. G. Shapiro, "Morphological edge detection," IEEE J. Robotics Automat., vol. RA-3, pp. 142-155, Apr. 1987.

[4] D. Marr and E. Hildreth, "Theory of edge detection." Proc. Rry. Soc. London, Ser. B, vol. 207, pp. 187-217, 1980.

[5] D. Talton, "Implementation of a Gaussian-smoothed gradient-edge operator," Dep. Elec. Eng., Univ. Pennsylvania, Tech. Rep. MS-CIS-85-12, 1985.

[6] T. Elfving, J.-0. Eklundh, and S. Nyberg, "Edge detection using the Marr-Hildreth operator with different sizes," in Int. Con$ on Pattern Recognition, 1982, pp. 1109-1 112.

[7] J. Canny, "A computational approach to edge detection," IEEE Trans. Pattern Anal. Machine Intell., vol. PAMI-8, pp. 679-697, Nov. 1986.

[8] V. Torre and T. A. Poggio, "On edge detection," IEEE Trans. Pattern Anal. Machine Intell., vol. PAMI-8, pp. 147-163, Mar. 1986.

[9] F. M. Dickey, K. S. Shanmugam, and J. A. Green, "An optimal frequency domain filter for edge detection in digital pictures," IEEE New York: Wiley, 1978.

[10] J. W. Modestino and R. W. Fries, "Edge detection in noisy images using recursive digital filtering," Comput. Graphics Image Processing, vol. 6, pp. 409-433, 1977.

[11] R. Nevatia and K. R. Babu, "Linear feature extraction and description," *Comput. Graphics Image ProcessinR,* vol. 13, pp. 257-269. 1980

[12] L. D. Andrews and S. Sinclair, "Macro-vascular topography in diabetic retinopathy: Analysis of fundus pictures using high resolution digital image processing," in ARVO Abstract, p. 262, 1988.

[13] M. Tanaka and K. Tanaka, "An automatic technique for fundus photograph mosaic and vascular net reconstruction," in MEDlNFO '80. Amsterdam, The Netherlands: North-Holland, 1980. pp, I 16-120.

[14] Y. Okamoto, S. Tamura, and K. Yanashima, “Zero-crossing interval correction in tracing eye-fundus blood vessels,” Pattern Recognition, vol. 21, pp. 227-233, 1988.
[15] S. Yamamoto and H. Yokouchi, “Automatic recognition of color fundus photographs,” in Digital Processing o j Biomedical Images. New York: Plenum, 1976, pp. 385-397.
[17] S. Chaudhuri, S. Chatterjee, N. Katz, M. Nelson, and M. Goldbaum, “Detection of blood vessels in retinal images using two-dimensional matched filters,” IEEE Trans. Med. Imag., vol. 8, no. 3, pp. 263–269, 1989.
[18] T. Chanwimaluang, G. Fan , and S.R. Fransen, “Hybrid retinal image registration,” IEEE Trans. Inf. Tech. Bio., vol. 10, no. 1, pp. 129-–142, 2006.
[19] T. Chanwimaluang, and F. Guoliang, “An efficient blood vessel detection algorithm for retinal images using local entropy thresholding”. ISCAS (5) 2003,pp.21-24
[20] A.C. Kak, M. Slaney, Principle of Tomographic Imaging, IEEE Press, 1999
[21] L. Feldkamp, L. Davix, J. Kress, Practical Cone- beam Algorithm, J. Opt. Soc. Am., Vol. A1, pp. 612–619, 1984
[22] B. Robbin, J. Nichols, R.L. Mokwa, B. Khun, M.M. Maclaughlin, and N. Hudyma, “Quantifying Internal Macroporosity using CT Scanning,” *ARMA* 11-264
[23] N. Hudyma, K. Johnson, C. Sherman, and M. Maclaughlin, “Comparisons of 2D Imaging Techniques for Internal Macropores Characterization,”*ARMA*.10-376